This is a preprint, the final version is subject to change, of the American Mineralogist (MSA)
Cite as Authors (Year) Title. American Mineralogist, in press.
(DOI will not work until issue is live.) DOI: http://dx.doi.org/10.2138/am-2016-5518

TITLE

Ni-phyllosilicates (garnierites) from the Falcondo Ni-laterite deposit (Dominican Republic): mineralogy, nanotextures and formation mechanisms by HRTEM and AEM

AUTHORS AND AFFILIATIONS

Cristina Villanova-de-Benavent – cvillanovadb@ub.edu

Departament de Cristal·lografia, Mineralogia i Dipòsits Minerals, Facultat de Geologia, Universitat de Barcelona (UB), Martí i Franquès s/n, 08028 Barcelona, Spain. +34 934021341

Fernando Nieto – nieto@gr.es

Departamento de Mineralogía y Petrología and IACT, Universidad de Granada, CSIC, Av. Fuentenueva 18071 Granada, Spain. +34 609132940

Cecilia Viti – cecilia.viti@unisi.it

Dipartimento di Scienze Fisiche, della Terra e dell'Ambiente, Università degli Studi di Siena, Via Laterina 8, 53100 Siena, Italy. +39 0577233988

Joaquín A. Proenza – japroenza@ub.edu

Departament de Cristal·lografia, Mineralogia i Dipòsits Minerals, Facultat de Geologia, Universitat de Barcelona (UB), Martí i Franquès s/n, 08028 Barcelona, Spain. +34 934021351

Salvador Galí – gali@ub.edu

Departament de Cristal·lografia, Mineralogia i Dipòsits Minerals, Facultat de Geologia, Universitat de Barcelona (UB), Martí i Franquès s/n, 08028 Barcelona, Spain. +34 934021341

Josep Roqué-Rosell – jrrosell@lbl.gov

Advanced Light Source, Lawrence Berkeley National Laboratory, One Cyclotron Road, MS 15R0317 Berkeley, California 94720, USA. +1 510 486 7035

ABSTRACT

Ni-bearing magnesium phyllosilicates (garnierites) are significant Ni ores in Ni-laterites worldwide. The present paper reports a detailed TEM investigation of garnierites from the Falcondo Ni-laterite deposit (Dominican Republic). Different types of garnierites have been recognized, usually consisting of mixtures between serpentine and talc-like phases which display a wide range of textures at the nanometer scale. In particular, chrysotile tubes, polygonal serpentine and lizardite lamellae are intergrown with less crystalline, talc-like lamellae. Samples consisting uniquely of talc-like and of sepiolite-falcondoite were also observed, occurring as distinctive thin lamellae and long ribbon-shaped fibers, respectively. HRTEM imaging indicates that serpentine is replaced by the talc-like phase, whereas TEM-AEM data show preferential concentration of Ni in the talc-like phase. We suggest, therefore, that the crystallization of Ni-bearing phyllosilicates is associated with an increase in the silica activity of the system, promoting the replacement of the Ni-poor serpentine by the Ni-enriched talc-like phase. These results have interesting implications in material science, as garnierites are natural analogues of Ni-bearing phyllosilicate-supported synthetic catalysts. Finally, SAED and HRTEM suggest that the Ni-bearing talc-like phase corresponds to a variety of talc with extra water, showing larger d001 than talc (i.e. 9.2–9.7 Å), described as “kerolite”-“pimelite” in clay mineral literature.

KEYWORDS

Ni-laterites; garnierites; chrysotile; polygonal serpentine; lizardite; “kerolite”-“pimelite”; sepiolite-falcondoite; HRTEM

This is a preprint, the final version is subject to change, of the American Mineralogist (MSA)
Cite as Authors (Year) Title. American Mineralogist, in press.
(DOI will not work until issue is live.) DOI: http://dx.doi.org/10.2138/am-2016-5518

MANUSCRIPT

INTRODUCTION

Garnierite was originally the name of a mineral species discovered in 1863 in New Caledonia (Garnier 1867), although it was later proved to be a mixture of different Ni-hydrous silicates (e.g. Pecora et al. 1949, Faust 1966). Since then, the term garnierite has been widely used in the literature to refer to the group of green, fine-grained, poorly crystallized, Ni-bearing magnesium phyllosilicates, including serpentine, talc, sepiolite, smectite and chlorite, often occurring as mixtures (e.g. Faust 1966, Brindley and Hang 1973, Springer 1974, Brindley 1978, Wells et al. 2009, Villanova-de-Benavent et al. 2014a). Therefore, despite not being a valid mineral name, *garnierite* became a convenient field term used by mine geologists to designate all green Ni-phyllosilicates when a more specific characterization was not possible (Brindley 1978), and many authors have used this term with this general meaning (e.g. Moraes, 1935, Pecora and Hobbs 1942, Pecora et al. 1949, Varela 1984, Gleeson et al. 2003, 2004, Freyssinet et al. 2005, Wells et al. 2009).

In addition, the classification and naming of the garnierite minerals represents a complex, long-lasting controversy, because of their fine-grained nature, poor crystallinity and frequent occurrence as intimate mixtures of different mineral species (Brindley and Hang 1973). Brindley and co-authors, after various studies, distinguished the following Mg-Ni series: the serpentine group minerals i) lizardite-népouite and ii) chrysotile-pecoraite; iii) berthierine-brindleyite; the talc-like structures iv) talc-willemseite and v) “kerolite”-“pimelite”; vi) the chlorite series clinochlore-nimite; and finally vii) sepiolite-falcondoite (Brindley and Hang 1973, Brindley and Maksimović 1974, Brindley 1978, 1980). The most common garnierites found in nature are formed by lizardite-népouite and “kerolite”-“pimelite” (Brindley 1978), and many authors have been referred to them as “serpentine-like” (or “7 Å-type”) and “talc-like” (or “10 Å-type”) garnierites, respectively (e.g. Brindley and Hang 1973, Brindley and Maksimović 1974, Wells et al. 2009, Galí et al. 2012).

"Kerolite" and "pimelite" can be described as phases with talc affinity and extra water in their structure, within the ideal structural formula $(Mg,Ni)_3Si_4O_{10}(OH)_2 \cdot n(H_2O)$. Faust (1966) classified "pimelite" into the smectite group, although other authors proved that neither "kerolite" nor "pimelite" exhibit intracrystalline swelling (e.g. Kato 1961, Brindley and Hang 1973, Brindley 1978). Regardless being both discredited species by the Commission on New Minerals, Nomenclature and Classification of the International Mineralogical Association (CNMNC-IMA), these names have been used during the following decades (e.g. Gleeson et al. 2003, Freyssinet et al. 2005, Tauler et al. 2009, Wells et al. 2009, Galí et al. 2012, Villanova-de-Benavent et al. 2014a, Cathelineau et al. 2015) and are considered as valid species by the International Association for the Study of Clays (AIPEA). According to Dosbaba and Novák (2012), "kerolite" represents a fine crystalline, poorly ordered, hydrated variant of talc, from which it can be distinguished by its very broad peak at approximately 10 Å; from smectite it can be distinguished by the absolute lack of swelling at an ethylene glycol atmosphere (Brindley and Brown 1980).

The remarkable Ni content of garnierites makes them significant Ni ores in some Ni-laterite deposits, such as in the Falcondo deposit, in the Dominican Republic (e.g. Golightly 1981, Elias 2002, Gleeson et al. 2003, Freyssinet et al. 2005). In the Falcondo Ni-laterite, characterized by an Al-poor ultramafic protolith, five garnierite types were distinguished according to their color, mineralogy, textures and chemical composition (namely types I to V, Villanova-de-Benavent et al. 2014a, b): I) Ni-Fe-bearing serpentine-like, II) Ni-bearing mixture of serpentine-like and "kerolite"-"pimelite", III) Ni-dominant mixture of serpentine-like and "kerolite"-"pimelite", IV) "kerolite"-"pimelite", and V) sepiolite-falcondoite.

These previous results, obtained by means of X-ray powder diffraction (XRD), optical and scanning electron microscopy (SEM, with energy dispersive spectrometry, EDS) and electron microprobe (EMP), indicated that, in general, the garnierites from Falcondo are complex mixtures at the

nanometer scale (Villanova-de-Benavent et al. 2014a, b). Although the methods used are sufficient for a description of the phases from an economic point of view, a detailed study including textures at the nanometer scale is necessary, to unravel the characteristics of the various mixtures and to gain further insight into the distribution of Ni.

Transmission Electron Microscopy (TEM) is a powerful technique to study the mineralogy, chemistry, and textural features of phases which commonly occur as poorly crystalline, fine grained mixtures at the nanometer scale. It has been extensively used to study phyllosilicates and, in particular, this method allows distinction of the different minerals of the serpentine group (e.g. Baronnet and Devouard 2005, Andréani et al. 2008, Suárez et al. 2011, Mellini 2014).

Serpentine group minerals are 1:1 trioctahedral phyllosilicates that develop different structural forms because of a geometrical misfit between tetrahedral and octahedral sheets. The three most common varieties are i) lizardite planar lamellae, ii) chrysotile tubes and iii) antigorite modulated structures. In addition, other microstructures may be found, such as polygonal serpentine, which develop sectored rolled fibers, larger than chrysotile tubes, with 15 or 30 sectors separated by 24º and 12º, respectively (e.g. Baronnet and Devouard 2005, Andréani et al. 2008, Mellini 2014, and references therein). Up-to-date studies report that sectors are actually composed of lizardite (e.g. Mellini 2014).

However, a limited number of exhaustive TEM works on Ni-bearing Mg-phyllosilicates exists up to the present (Uyeda et al. 1973, Esson and Carlos 1978, Poncelet et al. 1979, Pelletier 1983, Soler et al. 2008, Tauler et al. 2009, Suárez et al. 2011), and high resolution imaging and electron diffraction studies are in general scarce. Furthermore, most of these publications are based on crushed and dispersed material onto TEM grids, omitting the textural information of the assemblages and the relationships between different phases.

This paper presents a textural and chemical characterization by TEM of the different garnierites described in the Falcondo Ni-laterite deposit. The aim of this work was to describe the textural

relationships between the different garnierite-forming minerals and to determine the distribution of Ni at the nanometer scale based on High Resolution TEM (HRTEM) and Analytical Electron Microscopy (AEM).

GEOLOGICAL SETTING AND GARNIERITE OCCURRENCE

Hydrous silicate Ni-laterites of the Falcondo deposit are developed on the Loma Caribe, an ophiolitic peridotite belt in the Cordillera Central in the Dominican Republic. This belt consists of an elongated body, 4–5 km wide and 95 km long, oriented NW-SE and bounded by major faults (Fig. 1a, b). The Loma Caribe ultramafic rocks, formed in the upper mantle, are composed of harzburgites, dunites and lherzolites, partially altered to serpentinites during their emplacement to the present day tectonic position (Lewis et al. 2006, Proenza et al. 2007). Partially serpentinised peridotites have been exposed to weathering and erosion since the early Miocene, when the laterisation process began (Lewis et al. 2006).

The Falcondo Ni-laterite profile is up to 60 m thick and is divided into two main zones or horizons: the limonite on the top and the saprolite at the bottom (Fig. 1c; Haldemann et al. 1979, Lithgow 1993, Lewis et al. 2006). However, the contacts between subzones and their thicknesses vary vertically and laterally in all outcrops of the Falcondo deposit (Lewis et al. 2006, Aiglsperger et al. 2014, Villanova-de-Benavent et al. 2014a).

Garnierites in the Falcondo Ni-laterite occur mainly as mm-cm vein infillings in fractures, as thin coatings on joints and along fault planes, and as clasts and/or cements in different kinds of breccias. They are usually found within the lowermost part of the saprolite horizon, but may also be located near the unweathered serpentinized peridotite rocks, at the base of the lateritic profile, and in the upper saprolite horizon (Tauler et al., 2009, Villanova-de-Benavent et al. 2014a).

MATERIALS AND METHODS

Forty samples from the lower saprolite horizon containing different garnierite types were previously identified by X-ray powder diffraction (XRD), observed by optical and scanning electron microscopy (SEM-EDS), and analyzed by electron microprobe (EMP) at the Centres Científics i Tecnològics of the Universitat de Barcelona (CCiT-UB) (Villanova-de-Benavent et al. 2014a). From these forty samples, nine were selected as the most representative to be studied by transmission electron microscopy for the present work (Table 1). Three different methods of specimen preparation were combined, due to the difficulties posed by the friability of the material, and twelve grids were prepared with similar outcomes.

First, some samples were prepared as polished thin sections with Canada balsam. Representative areas containing garnierites to be studied by TEM were selected under the optical microscope. Copper grids were attached on the thin section including the areas of interest, and they were later detached, ion-thinned by a Gatan 600 ion mill and a Gatan PIPS 691 at the Centro de Instrumentación Científica in the Universidad de Granada (CIC-UGR) (Suárez et al., 2011), and by a Gatan 600 Duo Mill at the Dipartimento di Scienze Fisiche, della Terra e dell'Ambiente of the Università degli Studi di Siena (UniSi). Second, small fragments of other selected samples were carefully separated by hand-picking, polished manually up to ~30 micrometers thick and glued to a copper grid. The grids were ion-thinned by a Fischione 1010 Low Angle Ion Milling & Polishing System and a Gatan PIPS 691 at the CCiT-UB. It is worth noting that the aforementioned specimen preparation methods preserve the original texture of the mineral phases. Third, other samples were separated by hand-picking, ground in an agate mortar, suspended with ethanol and put on a copper grid in order to obtain additional, higher quality EDX analyses (e.g. López Munguira and Nieto 2000, Abad et al. 2001). Both ion-milled samples and powders were carbon-coated prior to the TEM study.

The TEM study was performed by Philips CM20 (CIC-UGR) and a Jeol JEM2010 (UniSi), equipped with Energy Dispersive X-ray spectrometer detectors (EDS-Oxford Isis, respectively) and operating at 200 kV. Additional images and electron diffraction patterns were obtained using a Jeol JEM2100 at 200 kV (CCiT-UB) as well.

Atoms per formula unit (apfu) were calculated from the atomic concentrations obtained by AEM and based on the theoretical number of positive charges of each mineral (14, 22 and 32 for serpentine, talc and sepiolite, respectively). Fe was calculated as Fe^{3+}, following Villanova-de-Benavent et al. (2014a) and according to the Fe^{2+}/Fe^{3+} XANES maps obtained in equivalent samples (Roqué-Rosell et al. submitted).

RESULTS

TEM results are shown in Figures 2-7, including a photograph of the selected sample (Figs. 2a-6a), a photomicrograph of the ion thinned specimen (Figs. 2b-6b), and low magnification, high resolution images and electron diffraction patterns. A comparison between the chemical compositions of the minerals obtained with TEM-AEM and EMP is shown in Figure 8, and AEM analyses are presented in Table 2.

Mineralogy and textures at the nano scale

Ni-bearing serpentine-dominant (type I). Type I garnierite consists of serpentine particles and minor talc-like bent thin lamellae with very little porosity (Fig. 2c). Serpentine occurs as tubes of various sizes which are randomly oriented, as basal and longitudinal sections are observed in low magnification images. There are two groups of serpentine tubes: i) thick, short tubes up to 5000 Å long and about 3000 Å diameter, with 85 Å in diameter hollow cores; ii) less abundant, narrow, long tubes up to 3000 Å in length and around 750 Å in diameter, with ~50 Å hollow cores (Fig. 2d). These nanostructures together with the particle size indicate that this sample is formed mostly by polygonal serpentine in relatively short fibers, finely intermixed with talc-like lamellae. Uyeda et al.

(1973) also reported short, stubby tubes with central holes in serpentine-like garnierites from Brazil, with an average width of 740 Å (4.4 wt.% NiO; serpentine-talc mixture with a talc fraction of 0.13), with less abundant ill-defined platy fragments, which may resemble the talc-like particles in type I garnierite (Fig. 2c, d).

As seen in Fig. 2d, the short tubes display bending at the fiber tip. These features have also been observed in polygonal serpentines coexisting with polyhedral serpentines by Andréani et al. (2008). In the high resolution images of the short tubes longitudinal sections 7.3 Å spacings are observed, in some cases presenting dislocations (Fig. 2e). The 7.3 Å spacings were confirmed in both the electron diffraction patterns and the Fast Fourier Transform obtained for the same short tubes, which displayed few reflections of the *h*0*l* plane that can be indexed with the clinochrysotile-$2M_{c1}$ 14 Å structure (Brindley and Brown 1980) (Fig. 2f). However, no high resolution images of the long tubes could be obtained due to electron beam damage. According to the total diameters and the measured spacings, the short, thick ones have approximately 200 T-O layers and the long, thin ones have 50 T-O layers.

Ni-bearing mixture of serpentine- and talc-like particles (type II). In the specimen of type II garnierite, serpentine particles, with characteristic 7.2 Å spacings, display various shapes and sizes and are found scattered in a matrix of talc-like bundles (Fig. 3c, d). Some serpentine basal sections have diameters around 5000 Å with tiny hollow cores, and are divided in 15 equidimensional sectors with an angle of 24º between adjacent (001) lattice planes, so-called polygonal serpentine (Fig. 3e). In some cases, polygonal sections are kidney-shaped, resembling the polyhedral serpentine of Andréani et al. (2008) (Fig. 3f). The inner diameter of some polygonal serpentines is similar to the outer diameter of the chrysotile basal sections in type I (Fig. 3g). Other serpentine particles display less rounded cylindrical fibers, probably corresponding to oblique sections of serpentine tubes, smaller than the polygonal fibers (up to 3000 Å in diameter), which are hollow-cored or contain

disordered layers in the centre, probably of a talc-like phase (Fig. 3g). Uyeda et al. (1973) also observed those features and mentioned that this material in the cores could be amorphous. Talc-like lamellae were also observed to concentrate in curved aggregates (Fig. 3h).

Ni-dominant mixture of serpentine- and talc-like particles (type III). Type III garnierites display long and bent lamellae with basal fringe spacings of 9.2–9.4 Å and 7.2–7.4 Å mixed in single particles (Fig. 4c-e), which are frequently parallel to each other (Fig. 4d-e). Lamellae of 7.2–7.4 Å spacings are curved, more regular and thicker (from six to sixteen 7.2–7.4 Å spacings) when compared to the 9.2–9.4 Å lamellae (four fringes mostly, and up to six) (Fig. 4c-e). This is supported by electron diffraction patterns, showing that the sample is composed of crystalline lizardite with a 7.2 Å spacing, coexisting with a lower crystallinity talc-like phase (Fig. 4f). No polygonal serpentine was found and only one basal and one longitudinal section of chrysotile tubes were observed in the specimen. Similar features involving ~7 Å and ~10 Å structures were observed in a garnierite from Oregon (18.6 wt.% NiO, Xtalc = 27 %) by Uyeda et al. (1973). These values differ from those of the type III garnierite (29–50 wt.% NiO and average Xtalc of 47 %, Villanova-de-Benavent et al. 2014a). Garnierites from New Caledonia shown by Pelletier (1983) and references therein also displayed comparable features.

Talc-like particles (type IV). The specimen containing Ni-"kerolite"-"pimelite" garnierites is very homogeneous, as it consists uniquely of sets of superimposed and/or plaited, thin, apparent lamellae with two to six basal spacings of 9.5–9.7 Å (Fig. 5c, d, e), confirmed by the absence of ~7 Å fringes in this specimen. Identical textures were observed in 10 Å-type garnierites from Brazil by Esson and Carlos (1978), in which no other crystalline phases were detected either. These Brazilian garnierites under the optical microscope display botryoidal features and coexist with silica, like type IV garnierites (Villanova-de-Benavent et al. 2014a). The small particle size, together with the wide and

diffuse rings observed in the electron diffraction patterns (typical of a random polycrystalline pattern), suggest that the sample may have low crystallinity (Fig. 5f).

Sepiolite-falcondoite (type V). The obtained TEM bright field images demonstrate the presence of Ni-rich sepiolite roughly oriented in fine ribbons with lengths above several hundreds of nanometers (Fig. 6c, d) and frequently enclosed within an amorphous silica matrix (Fig. 6b, c, e). The high magnification image in Fig. 6e shows a normal section of the fiber with the well defined (110) crystalline planes. This image allows measuring the 12 Å spacing typical of sepiolite-falcondoite (Post et al. 2007, Tauler et al. 2009).

Mineral chemistry at the nanoscale

The composition of garnierite-forming minerals obtained by AEM is represented in Fig. 7, compared to previous analyses obtained by EMP (Villanova-de-Benavent et al. 2014a), and in Table 2. The identification of the mineral species based on the lattice fringe spacing and that from the chemical composition were coherent. In addition, to increase the number of analysis of each mineral species, additional analyses were obtained on particles deposited on copper grids (e.g. López Munguira and Nieto 2000, Abad et al. 2001).

In general, Al is virtually absent in the Falcondo garnierites. Serpentine particles have low Ni, up to 0.2 apfu in type I and 0.6 apfu in type II; and yield remarkable amounts of Fe, 0.1–0.4 apfu in type I and up to 0.3 in type II garnierites. Type III compositions are actually mixed analyses of lizardite lamellae and the talc-like phase, with Ni contents ranging from 2.7 to 3.3 apfu and Al and Fe below detection limits. Talc-like analyses from all the studied garnierite types yield highly variable Ni contents, between 1.2 to 2.3 apfu (1.7 on average), and Al and Fe are generally low (up to 0.13 apfu Al, 0.03 on average; and up to 0.04 apfu Fe, <0.01 on average). In addition, Ni content in talc-like particles increases gradually from type I to type IV garnierites (Fig. 7).

AEM results plot within or near the compositional fields previously obtained through EMP in the same samples (Villanova-de-Benavent et al. 2014a), although type III mixtures and some analyses of type II serpentines still deviate towards the "kerolite"-"pimelite" series. Even if in most cases it was impossible to obtain pure analysis of the constituent phases of the mixture due to the very small size of the individual packets (e.g. Fig. 4c, d, e), the AEM spot size of tens of nanometers versus the EMP spot size of one micrometer gives unique results of the preferential partitioning of Ni in talc-like particles rather than in the associated serpentines. In summary, the higher spatial resolution of AEM analyses allowed better discrimination than EMP analyses, with slight deviations from the average composition obtained by EMP toward the respective constituent end-members (Fig. 7).

Finally, the EDS spectra in type V garnierite enabled distinction of the Ni-sepiolite ribbons from the surrounding matrix. The Ni-sepiolite fibers show a distinctive Ni and Mg content in addition to Si and O, and the presence of Si seems to be related not only with sepiolite but also with amorphous SiO_2 matrix. Ni contents varied from 1.2 to 2.2 apfu and Al and Fe were below detection.

DISCUSSION

Nanotextural variability of garnierite from the Falcondo Ni-laterite

As stated by Brindley (1978), most garnierites are a mixture of serpentine-like and talc-like phases, and previous TEM imaging studies reported the occurrence of some garnierites as intimate mixtures of 7.2–7.4 and 9.2–9.7 Å phases at the nanometer scale (e.g. Uyeda et al. 1973, Poncelet et al. 1979, Soler et al. 2008). Most garnierites from the Falcondo Ni-laterite deposit (Figs. 2-5) actually consist of mixtures of different relative proportions of serpentine and talc-like phases ("kerolite"-"pimelite"). TEM analysis distinguished a wide variety of textures and mineral species of the serpentine minerals in the different garnierite mixtures (chrysotile tubes in type I, polygonal serpentine in type II, lizardite lamellae in type III). In addition, TEM revealed the presence talc-like

281 particles in all the serpentine-bearing garnierites even when these had not been detected by XRD, as
282 in type I, probably due to their small quantity and low crystallinity.
283 Another characteristic feature is that 7.2–7.4 Å fringes occurred in large numbers, whereas 9.2–9.7
284 Å fringes occurred in smaller sets (as stated by Uyeda et al. 1973), suggesting a lower crystallinity of
285 talc-like phases, which is coherent with their broad peaks, or absence of them, in powder X-ray
286 diffraction (Villanova-de-Benavent et al. 2014a) and with the diffuse and weak ring-shaped electron
287 diffraction patterns in this study. Kato (1961) also reported that talc-like garnierites from New
288 Caledonia produced ring-shaped selected area electron diffraction (SAED) patterns whereas
289 serpentine-like phases gave single crystal diffraction patterns with well-defined spots. Furthermore,
290 Pelletier (1983) (and references therein) distinguished the electron diffraction pattern of the talc-
291 willemseite, with a regular structure, from the "kerolite"-"pimelite", showing concentric circles.
292 Other studies reported unspecified disordered regions in the TEM photomicrographs as well (e.g.
293 Uyeda et al. 1973, Brindley 1978, Esson and Carlos 1978).
294 Such low crystallinity of the talc-like phase could be related to specific conditions, such as very low
295 temperature, high water availability and/or high growth rate during crystallization. The fact that the
296 10 Å fringes are less regularly defined than the 7 Å ones, could be also explained by a variable
297 degree of hydration of their interlayers (Brindley and Hang 1973, Uyeda et al. 1973) and/or possible
298 volatilization phenomena under the TEM vacuum.
299 Finally, sepiolite-falcondoite occurs as an independent phase, never mixed with serpentine nor talc-
300 like garnierites. It displays the characteristic elongated ribbon shape of sepiolite, commonly related
301 to amorphous silica and/or quartz, but has a remarkably higher Ni content (26.8 wt.% NiO) when
302 compared to sepiolites examined under TEM in other localities (maximum 3.3 wt.% NiO in
303 Indonesia; Kuhnel et al. 1978).
304 **Preferential Ni concentration in the talc-like structure**

According to AEM, talc-like phases yield higher Ni concentrations than serpentine, which is coherent with the good correlation between Ni content and the talc fraction in the garnierites from Falcondo, as suggested by Galí et al. (2012) and Villanova-de-Benavent et al. (2014a), and by Soler et al. (2008), in the Loma de Hierro Ni-laterite (Venezuela). The higher resolution of the AEM with respect to EMP enabled distinction of the serpentine particles from the "kerolite"-"pimelite" lamellae (Fig. 7), despite it being difficult to obtain pure, single-phase analyses of talc-like or serpentine in type III. Therefore, the distribution of Ni between serpentine and talc-like phases in type III could not be well established because of its finer particle size.

Despite Uyeda et al. (1973) stating that there was no correlation between Ni content and morphology of the particles under TEM, and between proportions of platy and elongated particles and the number of serpentine-like and talc-like layers (equivalent to serpentine or talc fraction, respectively), other studies reported that Ni is mostly concentrated in talc-like phases (e.g. Esson and Carlos 1978, Poncelet et al. 1979). Besides, Vitovskaya and Berkhin (1968) also showed some low-magnification and electron diffraction patterns of what they described as Mg- and Ni-bearing "kerolites" (actually garnierite mixtures). They identified typical, tiny clinochrysotile tubes in Mg-"kerolite" (consisting predominantly of serpentine with Ni below detection limit), and scales with tiny tubes of clinochrysotile in the Ni-"kerolite" (mostly a 10 Å mineral with 11.3 wt.% NiO). Consequently in this case Ni was also related to a 10 Å phase. Furthermore, Poncelet et al. (1979) showed by EMP analyses and by heating experiments that most of the nickel was concentrated in the octahedral layer of the 10 Å phase, and not homogeneously distributed in the octahedral layer of both the 7 Å and 10 Å. During these experiments, metallic Ni particles were deposited onto the 10 Å flakes and rarely onto the serpentine fibers after heating the sample. In addition to these observations and interpretations, our AEM data confirm that the Ni was preferably contained in the talc-like phase. Possibly, the TOT talc structure is more likely to host Ni than the TO serpentine structure, as

329 demonstrated by the equilibrium constants of the simultaneous precipitation of Ni-serpentine and
330 "kerolite"-"pimelite" (Galí et al. 2012).
331 AEM results of garnierites from the Falcondo Ni-laterite showed that Ni concentration in serpentine
332 is lower than in the talc-like particles, and always below 50% of the total elements in octahedral
333 coordination. Therefore, neither népouite nor pecoraite, the Ni analogues of lizardite and chrysotile
334 respectively, are found in the garnierites from the Falcondo Ni-laterite deposit. However, the
335 presence of népouite and pecoraite is widely reported in other localities. In particular, népouite has
336 been extensively studied in New Caledonia (e.g. Brindley and Wan, 1975; Wells et al. 2009 and
337 references therein). One possible explanation for the different mineralogy between New Caledonian
338 and Dominican Ni-laterites is the lithology of the primary ultramafic rocks. In New Caledonia, the
339 protolith is mainly harzburgite and dunite (e.g. Pelletier, 1983, 1996), whereas in the Dominican
340 Republic the protolith is mostly clinopyroxene-rich harzburgite and lherzolite, commonly intruded
341 by microgabbro and dolerite dykes (e.g. Marchesi et al., 2012). The greater pyroxene content may
342 imply a greater availability of silica in the Falcondo Ni-laterite deposit, leading to the preferential
343 formation of talc rather than serpentine during weathering.
344 When examined under TEM, népouite usually occurs as highly crystalline plates (34.8 wt.% NiO,
345 Montoya and Baur 1963, 47.6 wt.% NiO, Manceau and Calas 1985), whereas pecoraite develops
346 coils and spiral shapes with three to five revolutions about the spiral axis (Faust et al. 1969, 1973,
347 Milton et al. 1983). In contrast, the serpentine particles in Falcondo present larger diameters and
348 lengths than the Ni-dominant counterparts described in the literature. Roy and Roy (1954) and
349 Milton et al. (1983) suggested that the substitution of Mg by Ni in chrysotile gives rise to non-
350 tubular but also not well formed, platy crystals. The Ni substitution probably prevents the tubes to
351 grow up to several hundreds of Å and to develop well rounded spirals or concentric tubes.
352 Accordingly, despite that the serpentine particles in type III were not analysed by AEM due to their

353 small particle size, the possibility of these serpentine lamellae yielding higher Ni contents than the
354 chrysotile tubes and polygonal serpentine in types I and II cannot be discarded.

355 **The formation mechanism of garnierites in the Falcondo Ni-laterite**

356 Low magnification and high resolution images are fundamental to understand the genetic
357 relationships between serpentine (in most cases, polygonal fibers) and Ni-rich, talc-like phases. The
358 talc-like lamellae are observed inside the serpentine central hole (Fig. 8a, b, e), surrounding the
359 serpentines, forming at the very edges of the particles (Fig. 8a, c, d, f) and at the boundaries between
360 adjacent sectors of the largest polygonal serpentines (Fig. 8e, f). In addition, HRTEM details indicate
361 that, at the reaction front, the (001) talc-like planes are parallel to the 001 serpentine ones. This
362 textural evidence suggests that talc-like phases form after serpentine, taking advantage of high stress
363 sites, such as the outer rims (where the basal planes of serpentine are bent), the fiber cores (highest
364 layer curvature), and the intersector boundaries. When replacement of serpentine by talc is more
365 advanced, sectors become fully pseudomorphed by talc-like lamellae (Fig. 8g, h) and talc-like
366 lamellae may develop rounded aggregates, mimicking the rounded shapes of former serpentine
367 particles (Fig. 8i, j). It is worth noting that these poorly crystalline, talc-like layers are bent and
368 characterized by extremely wide interlayer partings, giving rise to a highly porous nanotexture (Fig.
369 5d, e; 8h).

370 The overall data indicates that the formation of the successive phases in the garnierite mixtures may
371 be explained by an early formation of serpentine tubes. The diameter of the serpentine cores in type
372 II is comparable to the outer diameter of narrow chrysotile tubes in type I. This may indicate that the
373 diameter of the chrysotile increases in size until its curled structure is unstable. Then it is
374 transformed into polygonal serpentine while preserving a cylindrical core, which may more likely be
375 altered by later dissolution-precipitation than polygonal sectors. The serpentine particles are
376 subsequently replaced by “kerolite”-“pimelite”, starting from high stress sites and structural

discontinuities, such as cores, rims and contact between sectors. The final product is possibly a garnierite formed exclusively by talc-like lamellae (Fig. 9).

The later formation of "kerolite"-"pimelite" from serpentine particles is in accordance to the garnierite precipitation model proposed by Galí et al. (2012). This model is based on the assumption that in an Al-free system, such as the Falcondo laterite profile, the stability of serpentine, kerolite–pimelite or sepiolite–falcondoite is mainly controlled by the silica activity. As a result, the ideal formation of the Ni ore occurs as a successive precipitation of mineral phases progressively enriched in Ni and Si, because silica activity increases with time and through the profile. Thus, the first garnierite-forming phase to precipitate is serpentine, then followed by "kerolite"–"pimelite", and eventually by sepiolite–falcondoite and sepiolite–falcondoite with amorphous silica and/or quartz (Galí et al. 2012).

~~Conclusions~~

~~This work provides low and high resolution TEM images, showing that the five types of garnierites present characteristic features at the nanometer scale. Most consist of an ultrafine mixture of serpentine and a talc-like phases, but nanotextures and the relative amounts of serpentine and talc-like particles are variable from sample to sample.~~

~~Serpentine occurred as chrysotile tubes, polygonal serpentine and lizardite lamellae, and in general was more crystalline than the associated talc-like particles. We note that all garnierite samples contained at least a small portion of talc-like lamellae, even when this phase was not detected by XRD, due to its low crystallinity and/or low abundance. These particles, which could be the only component of garnierites, are in fact minerals of the "kerolite" "pimelite" series, a talc-like phase with extra water in their structure and showing an expansion of d_{001} spacing from 9.2 (talc) to 9.7 Å.~~

~~AEM data confirmed that Ni was mostly concentrated in "kerolite"-"pimelite" instead of in serpentine particles. Low magnification and HRTEM images established an insight of the~~

~~mechanisms by which Falcondo garnierites form, showing the preferential replacement of serpentine by "kerolite"-"pimelite" at high-stress sites in the serpentine structure, such as the inner walls of cores, outer rims and intersector boundaries.~~

IMPLICATIONS

The results obtained in this comprehensive TEM study on the garnierites from the Falcondo Ni-laterite deposit (Dominican Republic) reveal that the Ni-bearing serpentine, "kerolite"-"pimelite" and sepiolite-falcondoite components display a wide variety of textures and sizes at the nanometer scale. It is worth noting that most of the observed textures in Mg-serpentines (e.g. lamellae, chrysotile tubes, polygonal) are also found in their Ni-bearing analogues. However, the studied samples are characterized by low Ni contents in serpentines, whereas Ni is concentrated in the talc-like phases, reinforcing previous works (Villanova-de-Benavent et al., 2014). The results altogether provide further insight on the mineralogy of Ni-phyllosilicates as the highest grade Ni ores in a world-class hydrous silicate type Ni-laterite deposit.

The most noteworthy result of this work is the first evidence of replacement at the nanometer scale among garnierite-forming minerals. We have demonstrated that the Ni-enriched talc-like lamellae replace the polygonal serpentine and chrysotile tubes in the higher stress sites. In this model the Ni-enriched talc finally replaces the serpentine completely leaving some rolled and curved talc lamellae as remnants of the former serpentine (Fig. 9). This provides the direct proof that the crystallization of the Ni-bearing phyllosilicates at low temperature is associated with an increase in the silica activity of the system, which is coherent with previous observations at the micrometer scale (Villanova-de-Benavent et al., 2014) and the thermodynamic model for garnierites that predicted that Ni is preferably contained within the talc-like phase (Galí et al., 2012). As a consequence, Ni-enriched talc phases precipitate from already formed secondary serpentine particles. In the long term, in a more advanced stage of weathering, this will lead to the complete dissolution of serpentine particles

that will be entirely substituted by Ni-enriched talc-like and even sepiolite-like phases as the silica and Ni activity increase. In addition it is worth noting that this Ni-enrichment process leads to the formation of remarkable porosity in the material.

Therefore, the results of this work contribute to the knowledge of the formation of Ni-phyllosilicates under tropical conditions demonstrating that the Ni-poor serpentine particles are replaced by Ni-rich talc-like phases. This in turn has interesting implications in the field of material sciences. Recently (Sivaiah et al., 2011), synthesized Ni-containing serpentine-like and talc-like phyllosilicates were used as catalyst precursors for processing greenhouse gases (i.e. CO_2, CH_4). Thus the TEM characterization presented in this work also suggests that natural garnierites could be a good candidate to accomplish the requirements of a suitable catalyst precursor.

ACKNOWLEDGEMENTS

This research has been financially supported by the Spanish projects CGL2009-10924, CGL2012-36263, CGL2011-30153 and CGL2012-32169, the Catalan project SGR 2009-444, an FPU PhD grant sponsored by the Ministerio de Educación (Spain), and the "Estancias Breves" (Ministerio de Educación, Spain) and "Borsa de Viatges" scholarships (Universitat de Barcelona) to CVdB. The help and hospitality extended by the staff at Falcondo Glencore-Xtrata mine, especially by F. Longo and G. Bloise, are also gratefully acknowledged. Technical support by F. Mata, A. Villuendas (UB), I. Nieto, M.M Abad, J. D. Montes (CIC-UGR), C. Magrini and E. Mugnaioli (UniSi) was essential to this study. The authors want also to thank Professor J. F. Lewis, without whom the execution of the field work would not have been as profitable and instructive as it was. The careful and detailed revisions of the manuscript made by Mr. Alain Baronnet, Mr. Martin Wells and an anonymous reviewer increased the quality and accuracy of the text and are greatly acknowledged, as well as the supervision made by Mr. Keith D. Putirka and Mr. Warren Huff.

REFERENCES

Abad, I., Mata, M.P., Nieto, F., and Velilla, N. (2001) The phyllosilicates in diagenetic-metamorphic rocks of the South Portuguese Zone, southwestern Portugal. Canadian Mineralogist, 39, 1571-1589.

Aiglsperger, T., Proenza, J.A., Zaccarini, F., Lewis, J.F., Garuti, G., Labrador, M., and Longo, F. (2015) Platinum group minerals (PGM) in the Falcondo Ni-laterite deposit, Loma Caribe peridotite (Dominican Republic). Mineralium Deposita, 50, 105-123.

Andréani, M., Grauby, O., Baronnet, A., and Muñoz, M. (2008) Occurrence, composition and growth of polyhedral serpentine. European Journal of Mineralogy, 20, 159-171.

Baronnet, A., and Devouard, A. (2005) Microstructures of common polygonal serpentines from axial HRTEM imaging, electron diffraction and lattice-simulation data. Canadian Mineralogist, 43, 513-542.

Brindley, G.W. (1978) The structure and chemistry of hydrous nickel containing silicate and aluminate minerals. Bulletin du Bureau de Recherches Géologiques et Minières, section II, 3, 233-245.

Brindley, G.W. (1980) The structure and chemistry of hydrous nickel-containing silicate and nickel-aluminium hydroxy minerals. Bulletin de Minéralogie, 103, 161-169.

Brindley, G.W., and Brown, G. (1980) Crystal structures of clay minerals and their X-ray identification, 495 p. Mineralogical Society Monograph 5, London.

Brindley, G.W., and Hang, P.T. (1973) The nature of garnierite: I. Structure, chemical compositions and color characteristics. Clays and Clay Minerals, 21, 27-40.

Brindley, G.W., and Maksimović, Z. (1974) The nature and nomenclature of hydrous nickel-containing silicates. Clay Minerals, 10, 271-277.

Brindley, G.W., and Wan, H.-M. (1975) Compositions, structures and thermal behaviour of nickel-containingminerals in the lizardite–népouite series. American Mineralogist, 60, 863–871.

Cathelineau, M., Caumon, M.C., Massei, F., Brie, D., Harlaux, M. (2015) Raman spectra of Ni-Mg kerolite: effect of Ni-Mg substitution on O-H stretching vibrations. Journal of Raman Spectroscopy. DOI: 10.10002/jrs.4746.

Dosbaba, M., and Novák, M. (2012) Quartz replacement by "kerolite" in graphic quartz-feldspar intergrowths from the Věžná I pegmatite, Czech Republic: a complex desilication process related to episyenitization.. Canadian Mineralogist, 50, 1609-1622.

Elias, M. (2002) Nickel laterite deposits—Geological overview, resources and exploration. In D. Cooke, and J. Pongratz, Eds., Giant Ore Deposits—Characteristics, Genesis, and Exploration, CODES Special Publication 4, p. 205–220. Hobart, University of Tasmania, Australia.

Esson, J., and Carlos, L. (1978) The occurrence, mineralogy and chemistry of some garnierites from Brazil. Bulletin du Bureau de Recherches Géologiques et Minières, section II, 3, 263-274.

Faust, G.T. (1966) The hydrous nickel-magnesium silicates – the garnierite group. American Mineralogist, 51, 33-36.

Faust, G.T., Fahey, J.J., Mason, B., and Dwornik, E.J. (1969) Pecoraite, $Ni_6Si_4O_{10}(OH)_8$, nickel analog of clinochrysotile, formed in the Wolf Creek meteorite. Science, 165, 59-60.

Faust, G.T., Fahey, J.J., Mason, B., and Dwornik, E.J. (1973) The disintegration of the Wolf Creek meteorite and the formation of pecoraite, the nickel analog of clinochrysotile. United States Geological Survey Professional Paper, 3480C, 107-135.

Freyssinet, Ph., Butt, C.R.M., and Morris, R.C. (2005) Ore-forming processes related to lateritic weathering. Economic Geology, 100th Anniversary Volume, 681-722.

Galí, S., Soler, J.M., Proenza, J.A., Lewis, J.F., Cama, J., and Tauler, E. (2012) Ni-enrichment and stability of Al-free garnierite solid-solutions: a thermodynamic approach: Clays and Clay Minerals, 60, 121-135.

Garnier, J. (1867) Essai sur la géologie et les ressources minérales de la Nouvelle-Calédonie. In Annales des mines, 6ème série, tome XII., 92 p. Dunod, Paris.

Gleeson, S.A., Butt, C.R., Elias, M. (2003) Nickel laterites: a review. Society of Economic Geologists Newsletter 54, 11–18.

Gleeson, S.A., Herrington, R.J., Durango, J., Velásquez, C.A., Koll, G. (2004) The mineralogy and geochemistry of the Cerro Matoso S.A. Ni laterite deposit, Montelíbano, Colombia. Society of Economic Geology 99, 1197-1213.

Golightly, J.P. (1981) Nickeliferous laterite deposits. Economic Geology, 75th Anniversary Volume, 710-735.

Haldemann, E.G., Buchan, R., Blowes, J.H., and Chandler, T. (1979) Geology of lateritic nickel deposits, Dominican Republic. In D.J.I. Evans, R.S. Shoemaker, H. Veltman, Eds., International Laterite Symposium, 4, p. 57-84. Society of Mining Engineers of the American Institute of Mining, Metallurgical, and Petroleum Engineers, New York.

Kato, T. (1961) A study on the so-called garnierite from New-Caledonia. Mineralogical Journal, 3, 107-121.

Kuhnel, R.A., Roorda, H.J., and Steensma, J.J.S. (1978) Distribution and partitioning of elements in nickeliferous laterites. Bulletin du Bureau de Recherches Géologiques et Minières section II, 3, 191-206.

Lewis, J.F., Draper, G., Proenza, J.A., Espaillat, J., and Jiménez, J. (2006) Ophiolite-Related Ultramafic Rocks (Serpentinites) in the Caribbean Region: A Review of their Occurrence, Composition, Origin, Emplacement and Ni-Laterite Soils Formation. Geologica Acta, 4, 237-263.

Lithgow, E.W. (1993) Nickel laterites of central Dominican Republic Part I. Mineralogy and ore dressing. In R.G. Reddy, R.N. Weizenbach, Eds., The Paul E. Queneau International Symposium,

519 Extractive Metallurgy of Copper, Nickel and Cobalt, Volume I: Fundamental Aspects, p. 403-425.
520 The Minerals, Metals and Materials Society, Portland.
521 Lopez Munguira, A, and Nieto, F. (2000) Transmission Electron Microscopy study of very low-
522 grade metamorphic rocks in Cambrian sandstones and shales. Ossa-Morena Zone. South-West
523 Spain. Clays and Clay Minerals, 48, 213-223.
524 Manceau, A., and Calas, G. (1985) Heterogeneous distribution of nickel in hydrous silicates from
525 New Caledonia ore deposits. American Mineralogist, 70, 549-558.
526 Marchesi, C., Garrido, C.J., Proenza, J.A., Konc, Z., Hidas, K., Lewis, J.F., and Lidiak, E., (2012)
527 Mineral and whole rock compositions of peridotites from Loma Caribe (Dominican
528 Republic): insights into the evolution of the oceanic mantle in the Caribbean region. European
529 Geosciences Union General Assembly, Geophysical Research Abstracts 14, EGU2012–EGU12161.
530 Vienna, Austria.
531 Mellini, M. (2013) Structure and microstructure of serpentine minerals. In F. Nieto, K.J.T. Livi,
532 Eds., Minerals at the nanoscale, p. 153-179. European Mineralogical Union Notes in Mineralogy
533 (Mineralogical Society of Great Britain and Ireland), London.
534 Milton, C., Dwornik, E.J., and Finkelman, R.B. (1983) Pecoraite, the nickel analogue of chrysotile,
535 $Ni_3Si_2O_5(OH)_4$ from Missouri. Neues Jahrbuch für Mineralogie - Monatschefte, 11, 513-523.
536 Montoya, J.W., and Baur, G.S. (1963) Nickeliferous serpentines, chlorites and related minerals
537 found in two lateritic ores. American Mineralogist, 48, 1227-1238.
538 Moraes, L.J. (1935) Niquel no Brasil. Boletim Republica dos Estados Unidos do Brasil, 9, 168 p.
539 Nickel, E.H., and Nichols, M.C. (2009) Materials Data Minerals Database (Online). Available:
540 http://www.materialsdata.com. (accessed June 19, 2015). Livermore, California.
541 Post, J.E., Bish, D.L., and Heaney, P.J. (2007) Synchrotron powder X-ray diffraction study of the
542 structure and dehydration behavior of sepiolite. American Mineralogist, 92, 91-97.

Pecora, W.T., and Hobbs S.W. (1942) Nickel deposit near Riddle Douglas County, Oregon. United States Geological Survey Bulletin, 931-I, 205-225.

Pecora, W.T., Hobbs S.W., and Murata, K.J. (1949) Variations in garnierite from the nickel deposit near Riddle, Oregon. Economic Geology, 44, 13-23.

Pelletier, B. (1983) Localisation du nickel dans les minerais "garniéritiques" de Nouvelle-Calédonie. In D. Nahon, Ed., International Congress on Alteration Petrology, Sciences Géologiques Mémoires, 73, p. 173-183. Centre National de la Recherche Scientifique, Paris.

Pelletier, B. (1996) Serpentines in nickel silicate ore from New Caledonia. Australasian Institute of Mining and Metallurgy Publication Series - Nickel conference, 6/96, p. 197-205. Kalgoorlie, Western Australia.

Poncelet, G., Jacobs, P., Delannay, F., Genet, M., Gerard, P., and Herbillon, A. (1979) Étude preliminaire sûr la localisation du nickel dans une garnierite naturelle. Bulletin de Minéralogie, 102, 379-385.

Proenza, J.A., Zaccarini, F., Lewis, J., Longo, F., and Garuti, G. (2007) Chromite composition and platinum-group mineral assemblage of PGE-rich Loma Peguera chromitites, Loma Caribe peridotite, Dominican Republic. Canadian Mineralogist, 45, 211-228.

Roqué-Rosell, J., Villanova-de-Benavent, C., Proenza, J.A. (submitted) The accumulation of Ni in serpentines and garnierites from Falcondo Ni-laterite deposit (Dominican Republic) elucidated by means of μXAS. Geochimica et Cosmochimica Acta.

Roy, D.M. and Roy, R. (1954) An experimental study of the formation and properties of synthetic serpentines and related layer silicate minerals. American Mineralogist, 39, 957-975.

Sivaiah, M.V., Petit, S, Beaufort, M.F., Eyidi, D., Barrault, J., Batiot-Dupeyrat, C., Valange, S. (2011) Nickel based catalysts derived from hydrothermally synthesized 1:1 and 2:1 phyllosilicates as

precursors for carbon dioxide reforming of methane. Microporous and Mesoporous Materials, 140, 69-80.

Soler, J.M., Cama, J., Galí, S., Meléndez, W., Ramírez, A., and Estanga, J. (2008) Composition and dissolution kinetics of garnierite from the Loma de Hierro Ni-laterite deposit, Venezuela. Chemical Geology, 249, 191-202.

Springer, G. (1974) Compositional and structural variations in garnierites. Canadian Mineralogist, 12, 381-388.

Suárez, S., Nieto, F., Velasco, F., and Martín, F.J. (2011) Serpentine and chlorite as effective Ni-Cu sinks during weathering of the Aguablanca sulphide deposit (SW Spain). TEM evidence for metal-retention mechanisms in sheet silicates. European Journal of Mineralogy, 23, 179-196.

Tauler, E., Proenza, J.A., Galí, S., Lewis, J.F., Labrador, M., García-Romero, E., Suárez, M., Longo, F., and Bloise, G. (2009) Ni-sepiolite-falcondoite in garnierite mineralization from the Falcondo Ni-laterite deposit, Dominican Republic. Clay Minerals, 44, 435-454.

Uyeda, N., Hang, P.T., and Brindley, G.W. (1973) The nature of garnierites: II. Electron-optical study. Clays and Clay Minerals, 21, 41-50.

Varela, J.dD. (1984) La estructura de las garnieritas. Geología Colombiana, 13, 29-40.

Villanova-de-Benavent, C., Proenza, J.A., Galí, S., García-Casco, A., Tauler, E., Lewis, J.F., and Longo, F. (2014a) Garnierites and garnierites: Textures, mineralogy and geochemistry of garnierites in the Falcondo Ni-laterite deposit, Dominican Republic. Ore Geology Reviews, 58, 91–109.

Villanova-de-Benavent, C., Proenza, J.A., Galí, S., Nieto, F., García-Casco, A., Roqué-Rosell, J., Tauler, E., and Lewis, J.F. (2014b) Mineralogy of Ni-phyllosilicates in the Falcondo Ni-laterite deposit (Dominican Republic): A multiscale approach. Proceedings ot the twenty first meeting of the International Mineralogical Association IMA2014, 298.

589 Vitovskaya, I.V., and Berkhin, S.I. (1968) К вопросу о природе керолита (On the question of the
590 nature of kerolite). Kora Vyvetrivaniya, 10, 134-159.
591 Wells, M.A., Ramanaidou, E.R., Verrall, M., and Tessarolo, C. (2009) Mineralogy and crystal
592 chemistry of "garnierites" in the Goro lateritic nickel deposit, New Caledonia. European Journal of
593 Mineralogy, 21, 467-483.
594 Whitney, D.L., and Evans, B.W. (2010) Abbreviations for names of rock-forming minerals.
595 American Mineralogist, 95, 185-187.

596 **TABLE AND FIGURE CAPTIONS**

597

598 **Table 1.** Summary of the studied garnierite samples from the Falcondo Ni-laterite (Dominican
599 Republic). The talc fraction (Xtalc) in the serpentine-talc mixtures is calculated according to
600 Brindley & Hang (1973).
601 **Table 2.** Representative normalized AEM analyses performed on Falcondo garnierites in atoms per
602 formula unit (apfu).

603

604 **Figure. 1.** Geological map of the Falcondo Ni-laterite (a) after Haldemann et al. (1979), location of
605 the deposit in the Dominican Republic (b) and schematic profile of the Falcondo Ni-laterite (c)
606 modified from Lithgow et al. (1979), Lewis et al. (2006), Villanova-de-Benavent et al. (2014a).
607 **Figure. 2.** Type I garnierite as seen under the TEM (specimen LC-101): a) image of the sample, the
608 specimen was detached from the area in the red rectangle; b) detail of the hole in the grid under the
609 optical microscope (plane polarised light); c) low magnification images of the specimen showing
610 short serpentine tubes (Srp) and minor talc-like lamellae (Tlc); d) detail of a short serpentine tube
611 with a hollow core (red arrow), next to a long serpentine tube (yellow arrow); e) high resolution
612 image of the area in the rectangle in d) showing the typical basal spacings of serpentine minerals of

7.3 Å, and a dislocation marked with a white arrow; f) electron diffraction pattern of the serpentine tubes. All images were obtained in a CM20 (CIC-UGR).

Figure. 3. Type II as seen under the TEM (specimen LC-100B): a) image of the sample, the specimen was detached from the area in the red rectangle; b) detail of the hole in the grid under the optical microscope (plane polarised light); c) low magnification image of the specimen showing circular sections of serpentine (Srp) within a matrix of talc-like platelets (Tlc), including an electron diffraction pattern with distinctive 7.2 Å spots and a less crystalline phase; d) high resolution image of polygonal serpentine, showing the angle between sectors and the basal spacings; e) kidney-shaped sectored serpentine; f) serpentine tubes with large holes filled with talc-like lamellae; g) oblique section of serpentine tube, the central hole being altered to talc as in f), and curled up talc-like lamellae aggregate (lower left). All images were obtained in a CM20 (CIC-UGR).

Figure. 4. Type III as seen under the TEM (specimen GAR-2.2): a) image of the sample, the specimen was detached from the area in the red rectangle; b) detail of the hole in the grid under the optical microscope (plane polarised light); c-e) high resolution images showing the presence of 7.2–7.4 Å and 9.2–9.4 Å basal spacings; f) electron diffraction image showing a higher crystallinity 7 Å spacing coexisting with a less crystalline material. All images were obtained in a Philips CM20 (CIC-UGR).

Figure. 5. Type IV (kerolite-pimelite) as seen under the TEM (specimen LC-100B): a) image of the sample, the specimen was detached from the area in the red rectangle; b) detail of the hole in the grid under the optical microscope (plane polarised light); c) low magnification images of the specimen showing bundles of talc-like lamellae; d) high resolution images of talc-like lamellae; e) close-up of image d) displaying the typical basal spacings of talc-like minerals; f) electron diffraction image. All TEM images were obtained in a Philips CM20 (CIC-UGR).

636 **Figure. 6.** Sepiolite-falcondoite (type V) as seen under the TEM (specimen GAR-7v): a) image of
637 the sample, the specimen was detached from area in the red rectangle, b) detail of the hole in the grid
638 under the optical microscope (plane polarised light), c) low magnification image of the specimen
639 showing sepiolite ribbons in a matrix of amorphous silica (obtained in a Jeol 2010, CCiT-UB), d)
640 detailed view of criss-cross sepiolite ribbons (in a Philips CM20, CIC-UGR), e) detail of 12 Å
641 fringes of a Ni-sepiolite ribbon oriented normal to the beam, in the matrix of amorphous silica
642 (Philips CM20, CIC-UGR).

643 **Figure. 7.** Triangular diagram comparing AEM (circles, squares and triangles) with previous EMP
644 (fields). Compositional fields from Villanova-de-Benavent et al. (2014a). Abbreviations from
645 Whitney & Evans (2010) except falcondoite (Fal), kerolite (Ker), pimelite (Pim), pecoraite (Pec).

646 **Figure 8.** Replacement textures between Ni-phyllosilicates: a) sectored serpentine being replaced by
647 talc-like lamellae, with talc-like lamellae inside the serpentine core (b) and growing from the
648 serpentine edges (c) (sample LC-100AB-5); d) large 15-sectored polygonal serpentine, showing talc-
649 like lamellae inside the core and at the edges of sectors (e), and at the border (f) (sample LC-100AB-
650 5); g) polygonal serpentine being altered to talc-like lamellae; h) detail of (g) (sample 09GAR-2.1);
651 i-j) rolled talc-like lamellae recording textures of former serpentine particles (i: sample 09GAR-2.1;
652 j: LC-100AB-5). All these images were obtained in a Jeol 2010 (UniSi).

653 **Figure 9.** Replacement model which may explain the formation of Ni-enriched talc-like ("kerolite"-
654 "pimelite") lamellae from the alteration of Ni-poor serpentine particles (1a-3a) and HRTEM images
655 representative of each precipitation stage (1b-3b): early formation of polygonal serpentine and
656 chrysotile tubes (1a, 1b), which are subsequently replaced by talc-like lamellae mainly in the higher
657 stress sites (inner cores, outer rims, borders between sectors) (2a, 2b), leading to a complete
658 replacement of serpentine particles by talc-like, leaving some rolled and curved talc-like lamellae as

remnants of the former serpentine features (3a, 3b). The HRTEM images were obtained in a Jeol 2010 (UniSi): sample LC-100AB-5 (1b), sample 09GAR-2.1 (2b), sample LC-100AB-4 (2c).

This is a preprint, the final version is subject to change, of the American Mineralogist (MSA)
Cite as Authors (Year) Title. American Mineralogist, in press.
(DOI will not work until issue is live.) DOI: http://dx.doi.org/10.2138/am-2016-5518

Type	Mineralogy (XRD)	Structural formula (EMP) [number of analyses averaged]	Xtal
TYPE I	serpentine + traces kerolite-pimelite (type I)	$(Mg_{2.29}Ni_{0.25}Fe_{0.19})Si_{2.17}O_{5.53}(OH)_{3.27}\cdot 0.19H_2O$ [23]	0.19
TYPE I	serpentine + traces kerolite-pimelite (type I)	$(Mg_{2.34}Ni_{0.48}Fe_{0.15})Si_{2.48}O_{6.27}(OH)_{3.49}\cdot 0.25H_2O$ [16]	0.25
TYPE II	serpentine + minor kerolite-pimelite (type II)	$(Mg_{1.94}Ni_{1.02}Fe_{0.03})(Si_{2.56}Al_{0.04})O_{6.49}(OH)_{3.40}\cdot 0.30H_2O$ [23]	0.30
TYPE III	serpentine + kerolite-pimelite (type III)	$(Ni_{2.56}Mg_{0.43})Si_{2.97}O_{7.44}(OH)_{3.02}\cdot 0.49H_2O$ [27]	0.49
TYPE III	serpentine + kerolite-pimelite (type III)	$(Ni_{2.42}Mg_{0.56}Fe_{0.01})Si_{2.71}O_{6.81}(OH)_{3.28}\cdot 0.36H_2O$ [4]	0.36
TYPE IV	kerolite-pimelite (type IV)	$(Mg_{1.90}Ni_{1.09})Si_{3.89}O_{9.76}(OH)_{2.09}\cdot 0.91H_2O$ [4]	0.91
TYPE IV	kerolite-pimelite (type IV)	$(Mg_{1.72}Ni_{1.27}Fe_{0.01})Si_{3.84}O_{9.61}(OH)_{2.16}\cdot 0.92H_2O$ [17]	0.92
TYPE IV	kerolite-pimelite (type IV)	$(Ni_{1.95}Mg_{1.04})Si_{3.69}O_{9.24}(OH)_{2.30}\cdot 0.85H_2O$ [109]	0.85
TYPE V	sepiolite-falcondoite (type V)	$(Mg_{4.60\text{-}7.05}Ni_{1.01\text{-}2.39}Fe_{0\text{-}0.05})(Si_{11.75\text{-}12.75}Al_{0\text{-}0.02})O_{15}(OH)_2\cdot 6H_2O$ [30]	-
TYPE V	sepiolite-falcondoite (type V)	$(Mg_{3.42\text{-}5.15}Ni_{2.29\text{-}5.24}Fe_{0\text{-}0.02})(Si_{11.57\text{-}12.55}Al_{0\text{-}0.15})O_{15}(OH)_2\cdot 6H_2O$ [4]	-
TYPE V	sepiolite-falcondoite (type V)	$(Mg_{6.51\text{-}7.94}Ni_{0.34\text{-}0.58}Fe_{0.01\text{-}0.27})(Si_{11.46\text{-}12.32}Al_{0.01\text{-}0.03})O_{15}(OH)_2\cdot 6H_2O$ [16]	-

	Type I (Srp)	Type I (Srp)	Type I (Tlc)	Type I (Tlc)	Type II (Srp)	Type II (Srp)	Type II (Srp)	Type II (Tlc)	Type II (Tlc)
	LC-101 serp 1-2	LC-101 serp 1-8	LC-101 serp 1-10	LC-101 serp 1-11	LC-100B-Serp-12	LC-100B-Serp-15	LC-100B serp 3b-5	LC-100B-2 (SERP)-4	LC-100B-2 (SERP)-14
	14	14	22	22	14	14	14	22	22
	2.737	2.509	2.374	2.111	2.756	2.556	2.590	1.482	1.008
	0.000	0.000	0.000	0.000	0.266	0.094	0.000	0.000	0.054
	1.825	2.085	3.869	3.846	1.888	1.899	2.132	3.905	3.907
	0.000	0.000	0.000	0.000	0.000	0.000	0.000	0.000	0.000
	0.000	0.000	0.000	0.000	0.000	0.000	0.000	0.000	0.000
	0.000	0.000	0.000	0.000	0.000	0.000	0.000	0.000	0.000
	0.000	0.000	0.000	0.000	0.000	0.000	0.000	0.000	0.000
	0.386	0.160	0.158	0.072	0.023	0.305	0.067	0.018	0.018
	0.035	0.080	0.651	1.091	0.035	0.047	0.045	1.681	2.070
	3.158	2.750	3.183	3.273	2.814	2.908	2.702	3.182	3.097
	1.825	2.085	3.869	3.846	2.154	1.993	2.132	3.905	3.961

	type III	type III	type III	type IV	type IV	type IV	type V	type V	type V
	GAR-2.3B-3	GAR-2.3B-7	GAR-2.3B-8	LC-100B-4 (TLC)-2	LC-100B-4 (TLC)-5	LC-100B-4 (TLC)-12	GAR-7v-3	GAR-7v-6	GAR-7v-7
	22	22	22	22	22	22	32	32	32
	0.364	0.417	0.413	1.440	1.494	1.725	1.961	2.138	2.013
	0.000	0.000	0.000	0.000	0.000	0.000	0.000	0.000	0.000
	3.770	3.757	3.966	3.997	4.015	4.026	6.065	6.106	6.090
	0.000	0.000	0.000	0.000	0.000	0.000	0.000	0.000	0.000
	0.000	0.000	0.000	0.000	0.000	0.000	0.000	0.000	0.000
	0.000	0.000	0.000	0.000	0.000	0.000	0.000	0.000	0.000
	0.000	0.000	0.000	0.000	0.000	0.000	0.000	0.000	0.000
	0.000	0.000	0.000	0.000	0.000	0.000	0.000	0.000	0.000
	3.096	3.068	2.656	1.566	1.476	1.222	1.910	1.649	1.806
	3.460	3.485	3.069	3.007	2.971	2.948	3.871	3.787	3.819
	3.770	3.757	3.966	3.997	4.015	4.026	6.065	6.106	6.090

This is a preprint, the final version is subject to change, of the American Mineralogist (MSA)
Cite as Authors (Year) Title. American Mineralogist, in press.
(DOI will not work until issue is live.) DOI: http://dx.doi.org/10.2138/am-2016-5518

FIGURES

Figure 1.

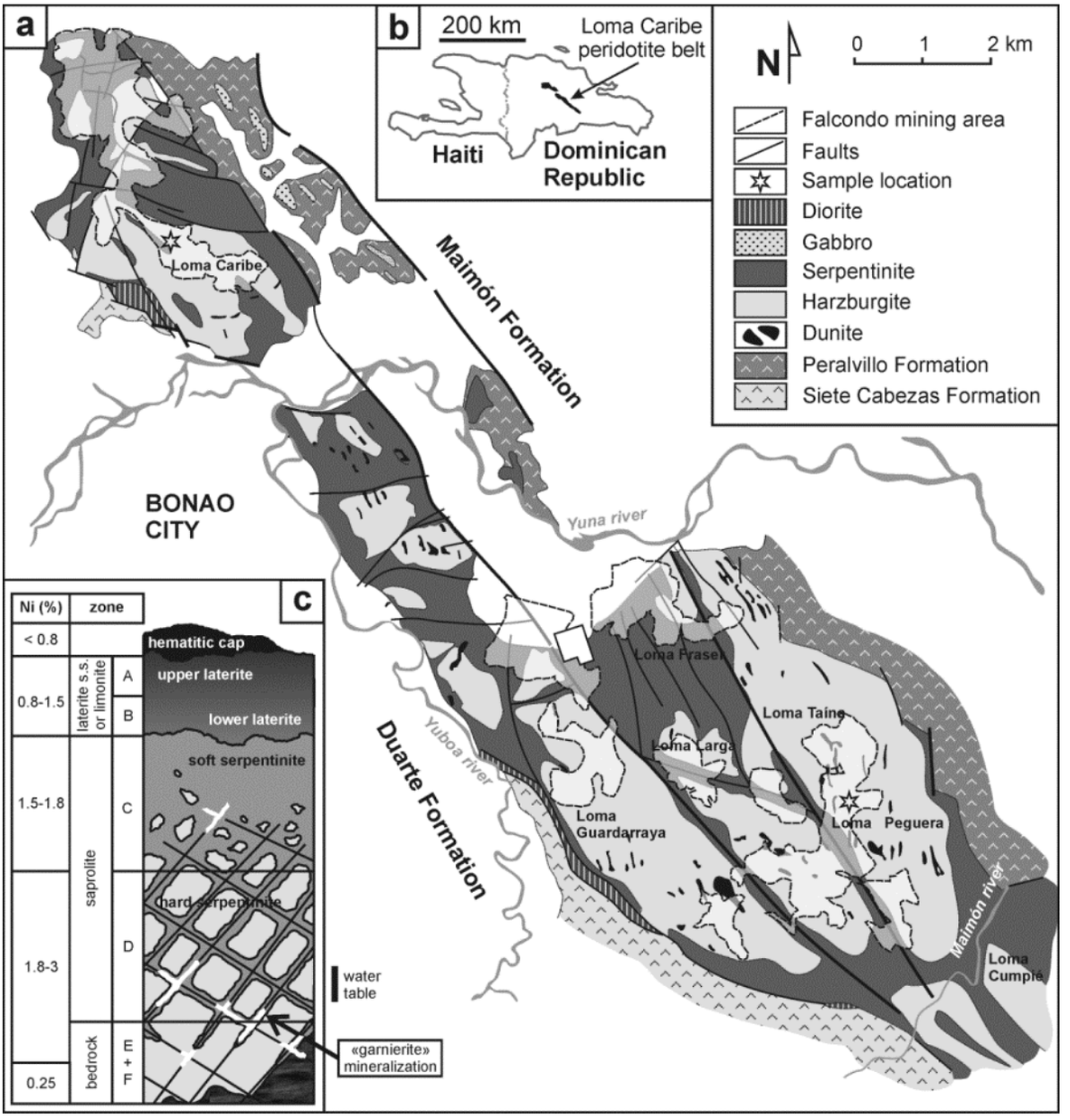

This is a preprint, the final version is subject to change, of the American Mineralogist (MSA)
Cite as Authors (Year) Title. American Mineralogist, in press.
(DOI will not work until issue is live.) DOI: http://dx.doi.org/10.2138/am-2016-5518

Figure 2.

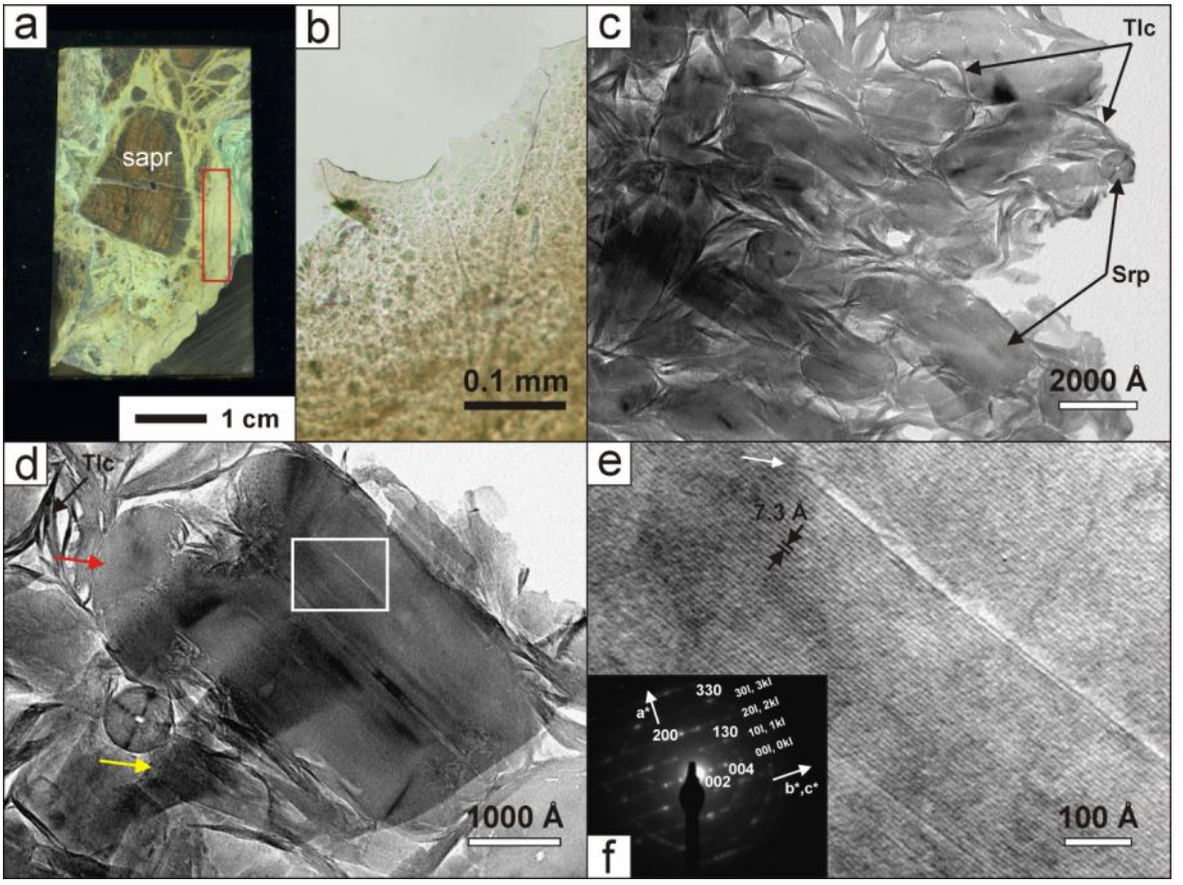

This is a preprint, the final version is subject to change, of the American Mineralogist (MSA)
Cite as Authors (Year) Title. American Mineralogist, in press.
(DOI will not work until issue is live.) DOI: http://dx.doi.org/10.2138/am-2016-5518

Figure 3.

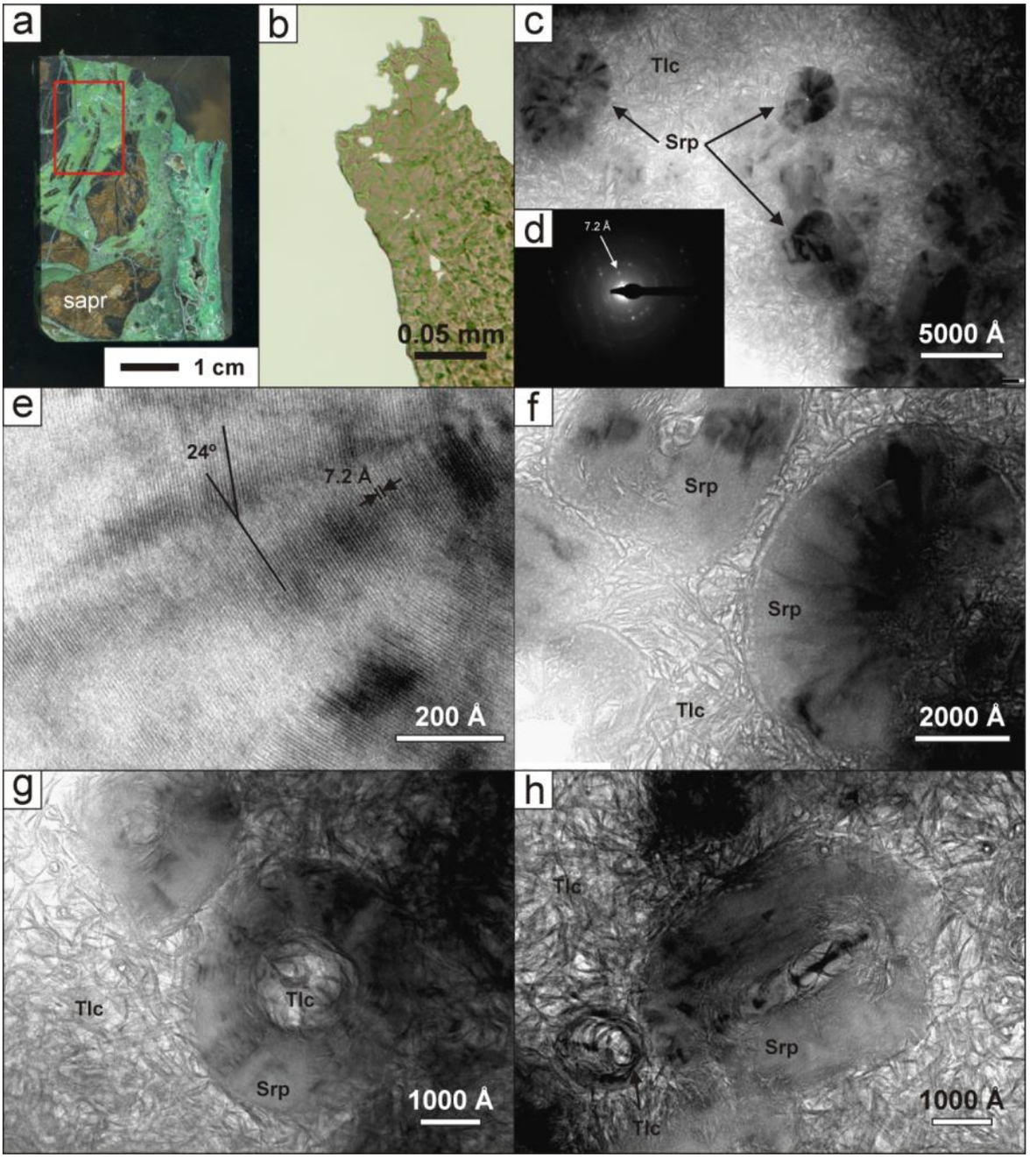

This is a preprint, the final version is subject to change, of the American Mineralogist (MSA)
Cite as Authors (Year) Title. American Mineralogist, in press.
(DOI will not work until issue is live.) DOI: http://dx.doi.org/10.2138/am-2016-5518

Figure 4.

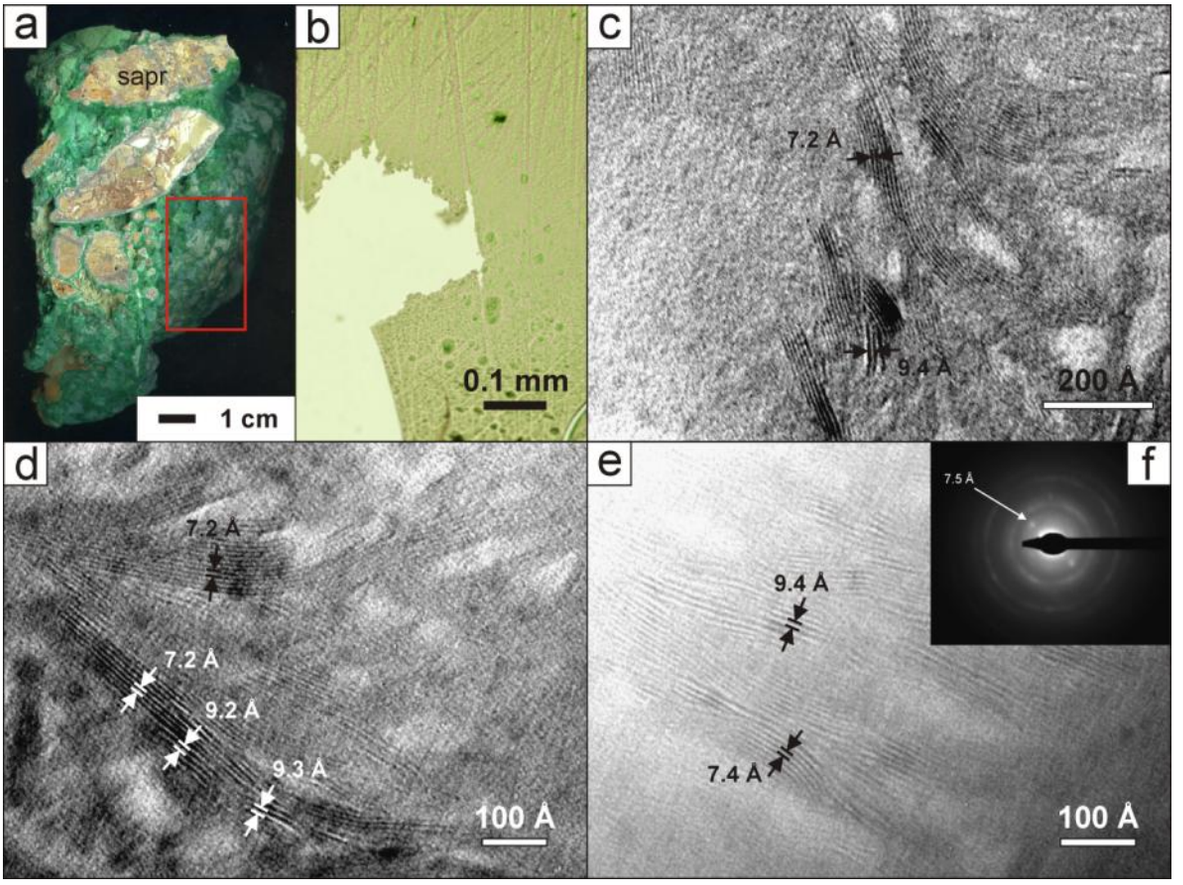

Figure 5.

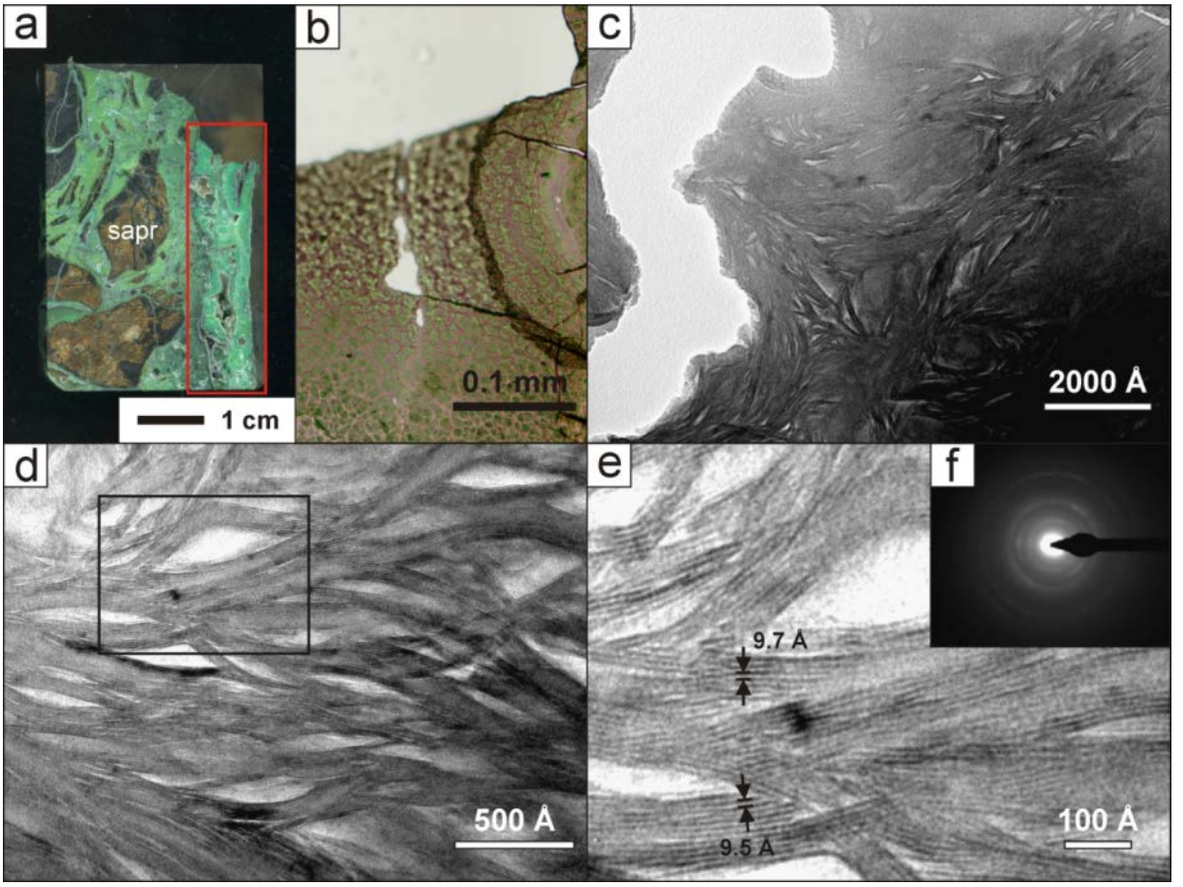

This is a preprint, the final version is subject to change, of the American Mineralogist (MSA)
Cite as Authors (Year) Title. American Mineralogist, in press.
(DOI will not work until issue is live.) DOI: http://dx.doi.org/10.2138/am-2016-5518

Figure 6.

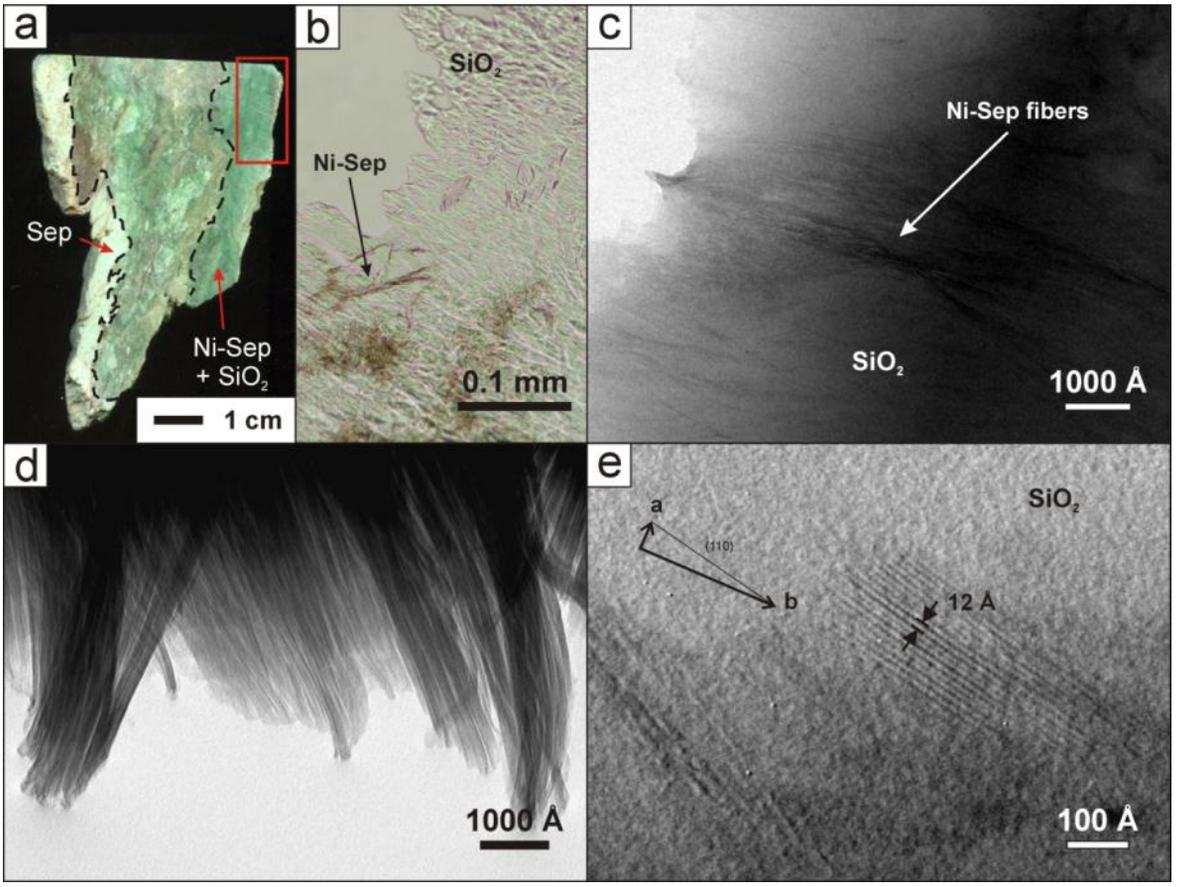

This is a preprint, the final version is subject to change, of the American Mineralogist (MSA)
Cite as Authors (Year) Title. American Mineralogist, in press.
(DOI will not work until issue is live.) DOI: http://dx.doi.org/10.2138/am-2016-5518

Figure 7.

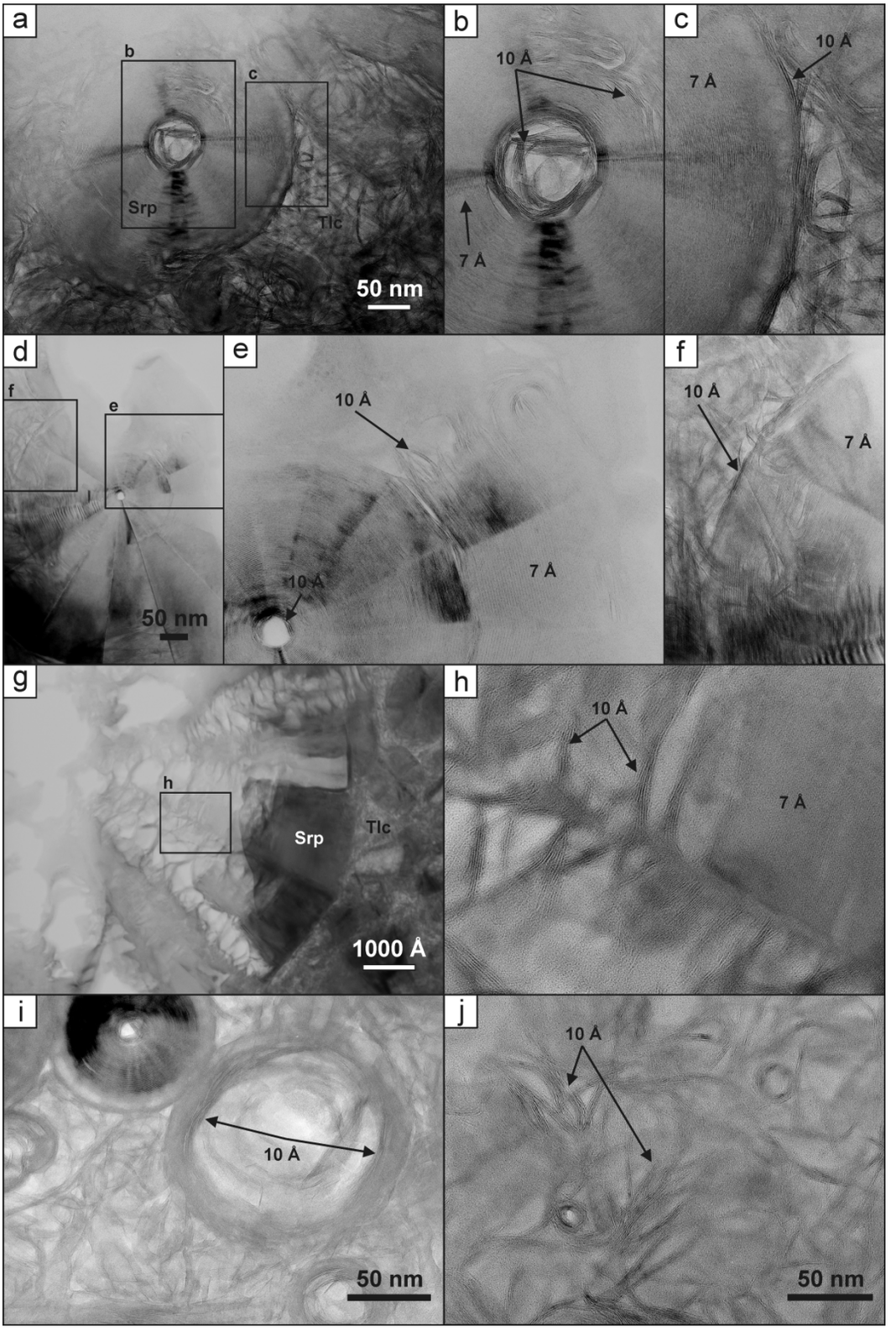

This is a preprint, the final version is subject to change, of the American Mineralogist (MSA)
Cite as Authors (Year) Title. American Mineralogist, in press.
(DOI will not work until issue is live.) DOI: http://dx.doi.org/10.2138/am-2016-5518

Figure 8.

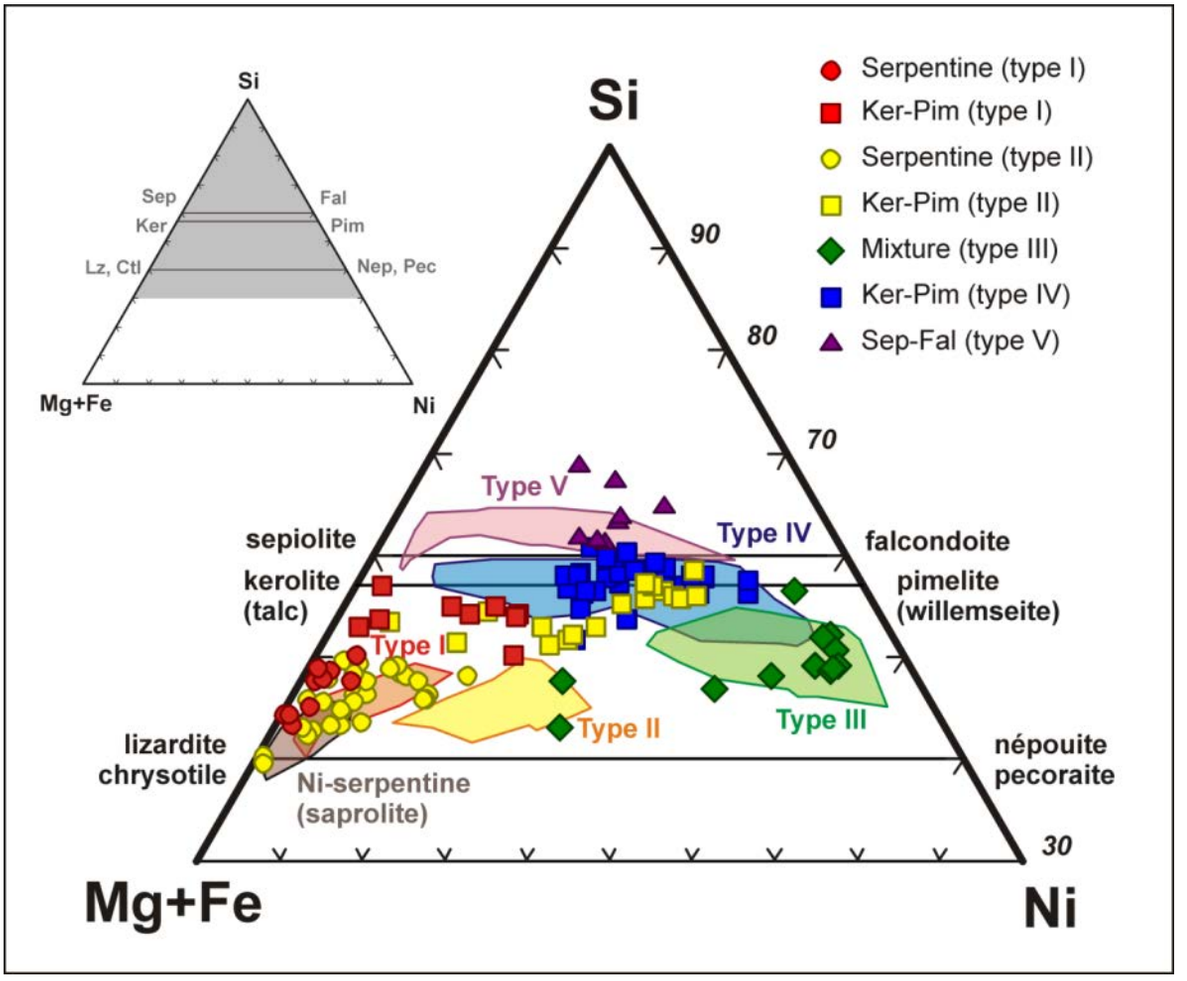

This is a preprint, the final version is subject to change, of the American Mineralogist (MSA)
Cite as Authors (Year) Title. American Mineralogist, in press.
(DOI will not work until issue is live.) DOI: http://dx.doi.org/10.2138/am-2016-5518

Figure 9.